remote sensing

MDPI

Article

Potential of UAS-Based Remote Sensing for Estimating Tree Water Status and Yield in Sweet Cherry Trees

Víctor Blanco [1,*], Pedro José Blaya-Ros [1], Cristina Castillo [2], Fulgencio Soto-Vallés [3], Roque Torres-Sánchez [3] and Rafael Domingo [1]

1 Dpto Ingeniería Agronómica, Universidad Politécnica de Cartagena (UPCT), Paseo Alfonso XIII, 48, E30203 Cartagena, Spain; pedro.blaya@upct.es (P.J.B.-R.); rafael.domingo@upct.es (R.D.)
2 Londonderry Maps, Parque Científico de Murcia, Complejo de Espinardo, Ctra. de Madrid, Km 388, E30100 Espinardo, Spain; cristina.castillo@londonderrymaps.com
3 Dpto Automática, Ingeniería Eléctrica y Tecnología Electrónica, Universidad Politécnica de Cartagena (UPCT), Campus de la Muralla s/n, E30202 Cartagena, Spain; pencho.soto@upct.es (F.S.-V.); roque.torres@upct.es (R.T.-S.)
* Correspondence: victor.blanco@upct.es; Tel.: +34-968-325-445

Received: 8 June 2020; Accepted: 21 July 2020; Published: 23 July 2020

Abstract: The present work aims to assess the usefulness of five vegetation indices (VI) derived from multispectral UAS imagery to capture the effects of deficit irrigation on the canopy structure of sweet cherry trees (*Prunus avium* L.) in southeastern Spain. Three irrigation treatments were assayed, a control treatment and two regulated deficit irrigation treatments. Four airborne flights were carried out during two consecutive seasons; to compare the results of the remote sensing VI, the conventional and continuous water status indicators commonly used to manage sweet cherry tree irrigation were measured, including midday stem water potential (Ψ_s) and maximum daily shrinkage (MDS). Simple regression between individual VIs and Ψ_s or MDS found stronger relationships in postharvest than in preharvest. Thus, the normalized difference vegetation index (NDVI), resulted in the strongest relationship with Ψ_s ($r^2 = 0.67$) and MDS ($r^2 = 0.45$), followed by the normalized difference red edge (NDRE). The sensitivity analysis identified the optimal soil adjusted vegetation index (OSAVI) as the VI with the highest coefficient of variation in postharvest and the difference vegetation index (DVI) in preharvest. A new index is proposed, the transformed red range vegetation index (TRRVI), which was the only VI able to statistically identify a slight water deficit applied in preharvest. The combination of the VIs studied was used in two machine learning models, decision tree and artificial neural networks, to estimate the extra labor needed for harvesting and the sweet cherry yield.

Keywords: artificial neuronal network; decision tree; DVI; NDVI; NDRE; OSAVI; water deficit

1. Introduction

Precision agriculture cannot be conceived without the recent evolution of technology. Technological tools such as soil–plant–atmosphere sensors and multispectral images obtained from unmanned aerial systems (UASs) are widely used to improve crop management. In recent years, several studies carried out in extensive crops and, to a lesser extend in woody crops, have reported promising results for UAS-based multispectral imagery for the remote sensing of crops and soil status as well as for detecting pests, diseases, and water and nutritional stress [1–4].

Multispectral aerial imagery is often used to calculate vegetation indices (VI) as combinations of the proportion of light reflected by leaves in the visible, red-edge, and near-infrared parts of the electromagnetic spectrum [5]. Among the most commonly used vegetation indices are the normalized

difference vegetation index (NDVI), the optimized soil adjusted vegetation index (OSAVI), the difference vegetation index (DVI), and the normalized difference red edge index (NDRE). NDVI is the most commonly used UAS-based index, is directly related to the chlorophyll content and plant health and, in horticultural crops and fruit trees, it has been reported to act as a robust water stress indicator. NDVI values range from −1 to +1: negative values refer to water bodies, 0 to barren land and dead plants (absence of green leaves), while positive values vary from light green leafy vegetation to +1, which indicates the highest possible density of healthy green leaves [6]. OSAVI avoids soil reflectance and reduces the influence of the soil which could be of interest in fruit trees [7]. DVI distinguishes between soil and vegetation, however, it does not account for the difference between reflectance and radiance caused by atmospheric effects or shadows [8]. Lastly, NDRE is used in those cases with dense vegetation when NDVI is saturated, since it is computed from the red edge band and it is able to measure deeper into the canopy [9]. Furthermore, a new vegetation index is proposed, the transformed red range vegetation index (TRRVI), which was developed using the high spectral resolution of the hyperspectral data at the "red" and "red edge" between 660 and 735 nm and the NDVI.

In woody crops such as nectarine, grapes, citrus, and almond, multispectral imagery has been seen to provide excellent results [5,10–13]. However, studies focusing on UAS imagery in sweet cherry trees are scarce despite the increase in their cultivation. Sweet cherry cultivation and production have increased worldwide by almost 25 % in the last 16 years, reaching 2.32 million tons, mainly in areas with a Mediterranean climate where water tends to be a scarce resource and therefore needs careful management to ensure sustainability [14]. In this respect, sweet cherry trees have been successfully grown using regulated deficit irrigation (RDI) strategies, which limit vegetative vigor and improve water use efficiency without penalizing fruit yield [15,16]. Sweet cherries are fast growing fruits. Hence, the preharvest period is described as a critical stage in which water stress might affect fruit development and penalize yield. Consequently, several studies have referenced postharvest (after flower differentiation period) as the best phenological stage to apply regulated deficit irrigation [15–17]. In order to assess the water status of sweet cherry trees, it was considered interesting to compare vegetation indices derived from multispectral images with conventional water stress indicators, such as the midday stem water potential, whose measurements are highly time-consuming and destructive but which is considered the most accurate plant water status indicator for sweet cherry trees [18–20]. Plant-based continuous indicators, like those derived from trunk and branch diameter variations (such as maximum daily branch shrinkage) have also shown promise for use in irrigation management for detecting water stress in several fruit crops [21,22]. Thus, the use of UAS-based indices might be a significant step forward, since they override one of the greatest limitations of conventional and continuous water stress indicators, the low number of trees that are usually measured and the need to extrapolate the results to a high number of trees growing over large areas.

Another potential application of the vegetation indices obtained by multispectral images is the possibility to use them as a parameter in leaf area and fruit yield estimation modelling [23–25]. In addition to these applications, the fruit harvesting time prediction could be a promising parameter to estimate in sweet cherry trees. The harvest process is manual and entails much human labor and money: the costs involved in hand-harvesting constitute more than 50% of the total costs of production [26]. Therefore, the ability to estimate crop load would help cherry growers in personnel management since cherry tree yields vary widely from year to year (alternate bearing). Traditionally, yield predictions are mostly made according to historical data and fruit set counts, which are not always accurate [27]. Consequently, predicting fruit yield would help growers to calculate the labor force needed for harvesting in a given year and thus facilitate decision-making.

Machine learning algorithms have recently been introduced in precision agriculture as they allow predictive models to be made that can help farmers improve their crop yields [28]. In those places where water is a limiting factor in production, several studies have been carried out with automatic learning algorithms to predict the water needs of crops following irrigation strategies, using soil and climate sensors [29] or UAS multispectral imagery [30]. Supervised algorithms such as decision

tree and artificial neural networks methods, can be used as classification or regression models for discrete/continuous estimation values such as the quantity of irrigation water needed for the following week [31] or for fruit yield prediction/classification as we propose in this work.

The overall aim of this paper was to ascertain the strengths and weaknesses of remote sensing indices obtained by multispectral imagery (UAS-based data) to detect the changes in canopy structure caused by water stress and to estimate the yield of adult sweet cherry trees. To achieve this goal, the response of remote structural indices (NDVI, OSAVI, DVI, OSAVI, and TRRVI spectroscopy) to two RDI treatments and a full irrigation treatment is compared with the response obtained by a conventional indicator (midday stem water potential) and a continuous indicator (maximum daily branch shrinkage).

2. Materials and Methods

2.1. Study Site

The study was conducted in a 0.50 ha experimental field of 17-year-old sweet cherry trees (*Prunus avium* L.) combination 'Prime Giant'/SL64, in the commercial orchard "Finca Toli" (38°8′ N; 1°22′ W, Elev. 680 m) located in Jumilla, Spain for two consecutive seasons, 2017 and 2018. Trees were trained to a Spanish bush (vase) system and spaced 5 m between rows and 3 m apart within the row. The soil is moderately stony and has a sandy loam texture with 67.5% sand, 17.5% silt, and 15% clay. The irrigation system consisted of a single drip line per tree row and three pressure-compensated emitters (4 L h^{-1}) per tree. The irrigation water was from a well, and had an average electrical conductivity ($EC_{25\,^{\circ}C}$) of 0.8 dS m^{-1}. Full bloom was in April and the harvest in June (2 June 2017 and 14 and 19 June 2018). The annual pruning was carried out approximately 60 d after harvest in accordance with the local growers' normal practice.

Daily climatic data, including crop reference evapotranspiration (ET_0), air temperature, air relative humidity, and rainfall, were recorded by an automatic weather station located 13 km from the experimental orchard owned by the Spanish Consultancy Service for Irrigation Users (SIAR; http://crea.uclm.es/siar/datmeteo/). From the temperature and humidity data, the vapor pressure deficit (VPD) was calculated according to Allen et al. [32].

2.2. Experimental Design

A completely randomized block experimental design with three irrigation treatments and four replicates (of seven trees each one) per treatment was established: a control treatment (CTL) and two regulated deficit irrigation treatments (RDI-1 and RDI-2). CTL was irrigated under non-limiting soil water conditions at 110% crop evapotranspiration (ET_c), while RDI-1 was irrigated at 90% ET_c during preharvest (slight water stress), 100% ET_c during flower differentiation (15–20 days after harvest, critical period) and 65% ET_c during postharvest (non-critical period) and RDI-2 was irrigated at 100% ET_c during preharvest and flower differentiation and 55% ET_c during postharvest (severe water stress). The irrigation dose was calculated using the formula $ET_c = ET_0 * K_c * K_r$, where K_c is the crop-specific coefficient for sweet cherry trees reported by Marsal [33] and K_r is a localization factor related to the percentage of ground covered by the crop [34].

2.3. Airborne Imagery

On 29 May and 1 August in 2017 and on 13 June and 21 August in 2018, four flight campaigns were carried out at noon. Aerial images were collected on sunny days with no noticeable wind by a multi-spectral camera (mod. Sequoia, Parrot Co. Ltd., Paris, France) of 1280 × 960 pixels equipped with GPS which was mounted on an unmannered aerial system (UAS mod. Phantom 3 Advance, DJI, Shenzhen, China). The multi-spectral camera captures images in four different bands of visible light: green, G: 550 nm center wavelength, 40 nm bandwidth; red, R: 660 nm, 40 nm; red edge, RE: 735 nm, 10 nm; near-infrared, NIR: 790 nm, 40 nm. The imagery was geo-processed to generate an orthomosaic

with the Pix4Dmapper Pro software (Pix4D SA, Lausanne, Switzerland). The flight altitude for the multispectral images was set at 50 m above ground level, which provided images with a ground resolution of 6.2 cm per pixel. From each image, trees were manually identified and their canopies were individualized to arrange them into circles of 2.5 m diameter, ensuring that only pure-vegetation tree crown pixels were chosen. Remote sensing indices were calculated with the open-software system Quantum Geographical Information System (QGIS 3.12 Bucuresti), using data from multiple reflectance bands. Remote vegetation indices NDVI, OSAVI, DVI, and NDRE were calculated using standard formulas from each processed UAS image mosaic [6–9]:

$$NDVI = (NIR - R)/(NIR + R) \quad (1)$$

$$OSAVI = (NIR - R)/[NIR + R + 0.16] \quad (2)$$

$$DVI = NIR - R \quad (3)$$

$$NDRE = (NIR - RE)/(NIR + RE) \quad (4)$$

In addition, a new index is proposed in this work:

$$TRRVI = [(RE - R)/(RE + R)]/[NDVI + 1] \quad (5)$$

NDVI, OSAVI, and DVI were computed in 2017 and 2018 (four flights); however, NDRE and TRRVI were only computed in 2018 (two flights).

2.4. Field Measurements

On the same day and at the same time as the UAS flight, midday stem water potential (Ψ_s, a conventional water status indicator) was measured with a Scholander pressure chamber (Model 3000, Soil Moisture Equipment, Santa Barbara, CA, USA) in six trees per treatment following the methodology proposed by McCutchan and Shackel [35]. The mature and healthy leaves selected were enclosed in black polythene bags and covered with aluminum foil for 2 h before the measurement. The branch diameter fluctuations of the same trees were recorded by dendrometers (LVDT sensors, model DF ± 2.5 mm, accuracy ± 10 µm, Solartron Metrology, Bognor Regis, UK). Each dendrometer was placed on the main tree branch away from direct sunlight. To prevent thermal expansion, the sensors were installed on holders made of invar and aluminum. From the branch diameter fluctuations, the maximum daily shrinkage (MDS) (continuous water status indicator) was calculated as the daily difference between the maximum and minimum branch diameters.

Vegetative growth was measured as the mass of pruning wood from each tree, which was individually weighed in the field using electronic scales (Scaltec Instruments GmbH, mod SSH91, Heiligenstadt, Germany). Similarly, in 2018 80 trees were selected at harvest and the individual yield of each tree was weighed to determine yield per tree.

2.5. Machine Learning Methodologies for Estimating Tree Crop Yield

Decision tree (DT) and artificial neural network (ANN) algorithms were used for harvesting prediction These types of algorithms have been widely used in the application of artificial intelligence techniques to the field of agriculture [36–39]. DT was performed using random forest as a classification model between two classes, normal labor predicted for harvesting (below a defined threshold of 40 kg tree^{-1}) and extra labor (above the threshold). ANN was implemented to provide sweet cherry tree yield estimation as a regression model, using the RStudio package (RStudio Inc., Boston, MA, USA). The software package used in the ANN analysis was 'neuralnet'.

Vegetation indices (VI) data were calculated from the UAS images taken during the preharvest flight in 2018 in 80 trees (predictor variables). Additional manual quantification data of the yield per tree was calculated for dataset development (response variable). The dataset was divided into

57 trees (71%) for training and 23 trees (29%) for testing, performing a cross-validation process based on the grouping of training and test sets following 10-fold cross-validation, which is considered useful when few data are available. This method increases the number of validations of the model for the same amount of data by crossing different subsamples of the same data [40]. The data were split into 10 equal parts (subsamples) used for the 10-fold cross validation. Each time, a different part was used as test set and the remaining nine parts were used as training set.

Performance values, such as precision, recall, and true positives, were calculated from the error matrix (confusion matrix).

Data from all the variables were scaled between 0 and 1 to improve convergence. This process is reversed in the predicted output of the model. Five features were used as input layer and two hidden layers with 3 and 4 neurons besides a bias neuron in each hidden layer. The model used a back-propagation algorithm which computed the gradients by iterating backwards. Root mean square error (RMSE) and the coefficient of determination were evaluated for gradient thresholding. Furthermore, for each pattern (actual and predicted) minimum and maximum values, standard deviation, coefficient of variation, and the normality tests Skewness and Kurtosis were calculated to ascertain any differences between both data distributions.

2.6. Statistical Analysis

The sensitivity analysis of the water stress indicators was calculated according to Goldhamer and Fereres [41] where sensitivity (S) is the result of the division of the signal intensity (SI) by the coefficient of variation (CV), and is always greater than 0. Analysis of variance (ANOVA), analysis of covariance (ANCOVA) and post-hoc test (Duncan's multiple ranges) with a significance level of $p < 0.05$ were performed using the statistical software package IBM SPSS Statistic 24 (IBM Corp., Armonk, NY, USA) and Statgraphics centurion XVI (StatPoint Technologies Inc., The Plains, VA, USA) in order to assess the effects of the imposed irrigation treatments on the response of conventional and continuous water status indicators, remote vegetation indices, and vegetative growth. The regression analysis was graphed and calculated with Microsoft Excel (Windows 10 Home, Microsoft Corp., Redmond, WA, USA) and SigmaPlot 12.5 (Systat Software Inc., San Jose, CA, USA).

3. Results

3.1. Environmental Conditions and Irrigation Water Applied

The weekly average reference evapotranspiration (ET_0) and vapor pressure deficit (VPD) and accumulated weekly precipitation recorded during the 2017 and 2018 seasons are summarized in Figure 1. Both VPD and ET_0 reflected the typical trend for Mediterranean climates both years of the study, with warm summers and mild winters.

Accumulated seasonal reference evapotranspiration from March to November reached close to 1000 mm both years of study, while the total rainfall recorded for the same period was 162 and 288 mm, for 2017 and 2018, respectively. In neither year did rainfall meet crop evapotranspiration levels, and irrigation was required; moreover, the rainfall pattern differed markedly between both years, with 124 mm falling during June–September (the period with the highest VPD values) in 2018, and 51 mm in 2017. The lower level of rainfall in 2017 than in 2018 led to a higher volume of irrigation water being applied, the volume of irrigation water decreasing by 10% in all irrigation treatments from 2017 to 2018 as a result. RDI-2 was the irrigation treatment needing the lowest amount of water in both years: 7% and 36% less water than RDI-1 and CTL, respectively. However, during preharvest, RDI-1 was the only irrigation treatment that applied deficit irrigation.

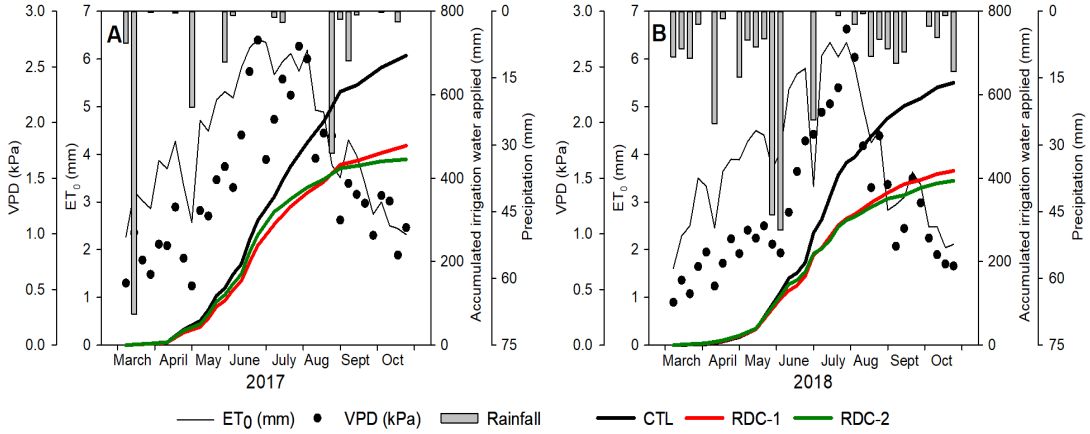

Figure 1. Seasonal evolution of weekly mean air vapor pressure deficit (VPD) and reference evapotranspiration (ET_0) and accumulated weekly precipitation and accumulated irrigation water applied to each treatment during the season 2017 (**A**) and 2018 (**B**) in the 'Prime Giant'/SL64 sweet cherry orchard in Jumilla (Spain).

3.2. Conventional and Continuous Plant Water Status Indicators and Remote Vegetation Indices

The plant water status indicators and VI provided different responses to the irrigation strategies assayed. Overall, conventional indicator (Ψ_s), continuous indicator (MDS) and remote VI (NDVI, OSAVI, DVI, NDRE, TRRVI) identified the water deficit applied to sweet cherry trees in the RDI-1 and RDI-2 treatments during postharvest compared with the trees irrigated to satisfy their water requirements (CTL). Figure 2 shows the NDVI maps taken from the orchard on two selected days in 2017, one day during preharvest and another day during postharvest.

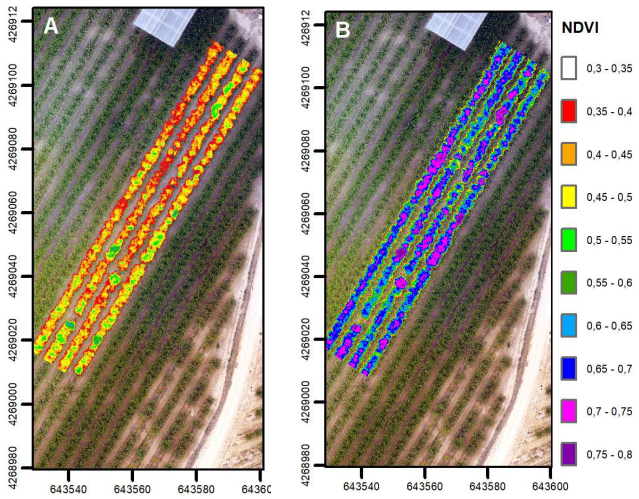

Figure 2. Normalized difference vegetation index (NDVI) distribution map of the sweet cherry orchard in 2017 preharvest (**A**) and postharvest (**B**).

Neither the OSAVI, nor the DVI were sufficiently sensitive to detect differences between CTL and RDI-1 any year of study, although DVI was able to identify significant differences between CTL and RDI-2 trees both years of study (Figure 3). In the postharvest of 2017, Ψ_s and NDVI were able to differentiate not only between CTL and RDI treatments, but also between RDI-1 and RDI-2 (Figure 3B,F). In 2017 postharvest, trees of all treatments had lower water status than in 2018, Ψ_s reaching mean values of −1.04 and −1.33 MPa for RDI-1 and RDI-2, respectively, compared with the −0.74 and −0.81 MPa reached for the same treatments in 2018. In the postharvest of 2018, Ψ_s was the only plant water status indicator that could significantly distinguish between RDI-1 and RDI-2.

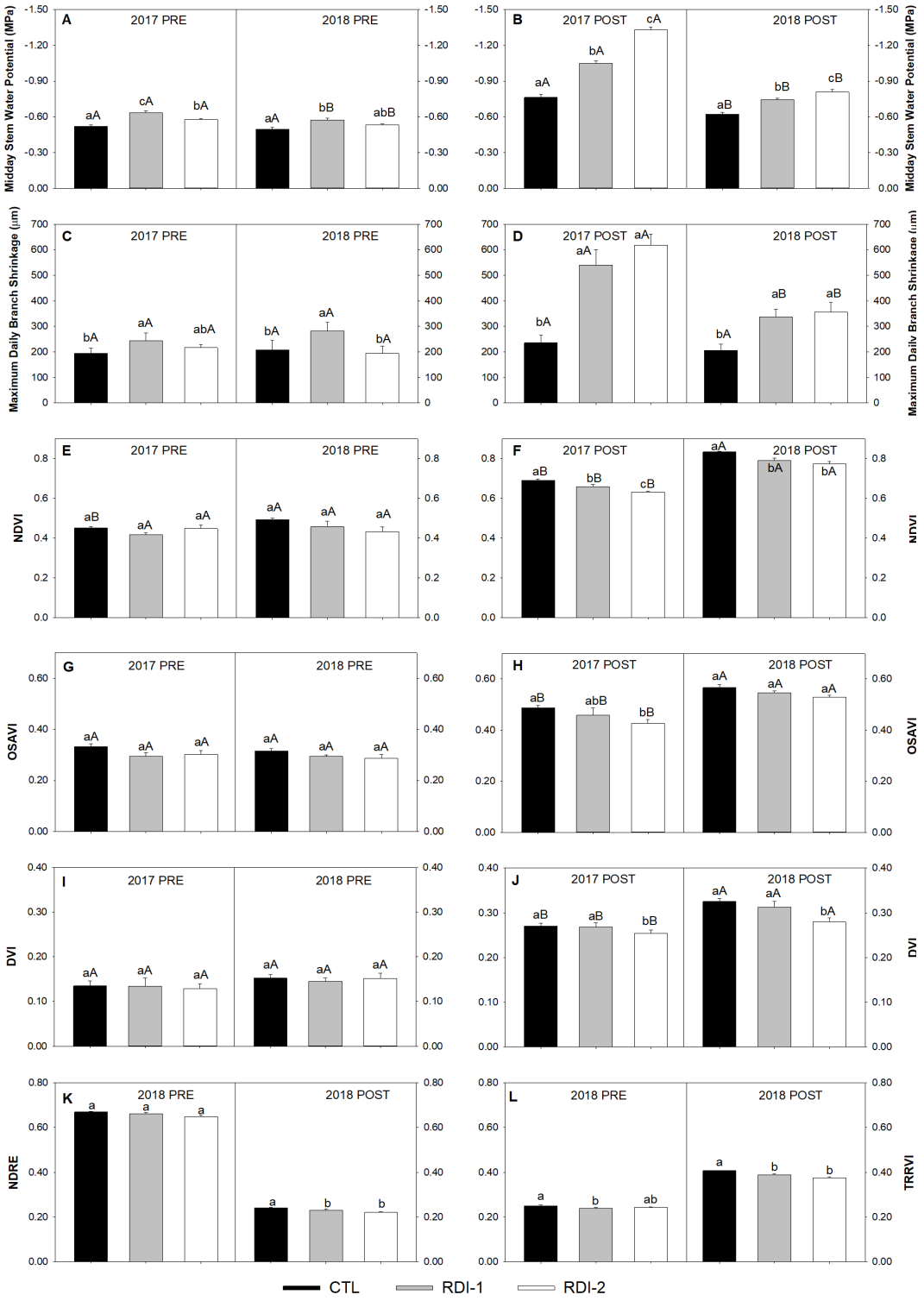

Figure 3. Mean values ± standard error of midday stem water potential (**A**,**B**), maximum daily branch shrinkage (**C**,**D**), normalized difference vegetation index (NDVI) (**E**,**F**), optimized soil adjusted vegetation (OSAVI) (**G**,**H**), difference vegetation index (DVI) (**I**,**J**), normalized difference red edge (NDRE) (**K**), and transformed red range vegetation index (TRRVI) (**L**) in preharvest (PRE) and postharvest (POST) flights for control (CTL)and regulated deficit irrigation treatments (RDI-1 and RDI-2). Lowercase letters indicate the statistical significance between irrigation treatments within the same year and capital letter indicate the statistical significance between years within the same treatment at $p \leq 0.05$ ($n = 6$).

On the other hand, in preharvest the response of the plant water status indicators and VI differed from that exhibited in postharvest. During the preharvest, only the sweet cherry trees of RDI-1 were submitted to water stress. The slight water stress applied to RDI-1 trees during preharvest led to significant differences in conventional (Ψ_s) and continuous (MDS) water stress indicators (Figure 3A,C). Among the remote indicators, only TRRVI was able to recognize the slight deficit applied. Neither NDVI, nor NDRE showed significant differences between RDI-1 and CTL trees during preharvest (Figure 3E,K), although both indicators were able to identify different levels of water stress, mid and strong, in the same trees during postharvest.

In order to compare the plant water status indicators and the VI, a sensitivity analysis was carried out (Table 1). The analysis showed that MDS was the plant water stress indicator with the highest SI (1.14 and 1.68, mean values for RDI treatments during preharvest and postharvest, respectively) followed by Ψ_s and NDRE. However, MDS was also the indicator that exhibited the highest CV (0.12–0.18), followed by OSAVI, which reduced its S as indicator. As regards the remote VI, and regardless of the irrigation treatment evaluated, NDRE showed the lowest variability and the highest sensitivity in preharvest. Furthermore, NDRE, OSAVI, and TRRVI resulted in higher signal intensity and sensitivity in preharvest than in postharvest (Table 1).

Table 1. Sensitivity analysis of the conventional, continuous plant water status indicators and remote vegetation indices (VI) for RDI-1 and RDI-2 in 2018 to preharvest and postharvest.

		Ψ_s		MDS		NDVI		OSAVI		DVI		NDRE		TRRVI	
		RDI 1	RDI 2	RDI 1	RDI 2	RDI 1	RDI 2	RDI 1	RDI 2	RDI 1	RDI 2	RDI 1	RDI 2	RDI 1	RDI 2
PRE	**SI**	1.15	1.07	1.36	0.93	0.93	0.88	0.88	0.88	0.97	0.93	0.99	0.98	0.95	0.96
	CV	0.07	0.04	0.12	0.15	0.15	0.14	0.07	0.12	0.24	0.20	0.02	0.03	0.04	0.03
	S	16.0	27.7	11.6	6.2	6.21	6.5	15.2	9.3	4.9	4.7	48.0	36.4	24.9	32.7
POST	**SI**	1.19	1.29	1.63	1.72	0.95	0.93	0.95	0.90	0.98	0.90	0.96	0.92	0.95	0.92
	CV	0.05	0.06	0.16	0.18	0.03	0.04	0.19	0.12	0.09	0.08	0.05	0.03	0.05	0.04
	S	25.7	20.9	10.4	9.4	28.5	22.5	13.2	8.3	10.4	12.1	19.3	28.0	19.4	21.3

Water status indicators: Ψ_s (midday stem water potential), MDS (maximum daily branch shrinkage). Vegetation indices: NDVI (normalized difference vegetation index), OSAVI (optimized soil adjusted vegetation index), DVI (difference vegetation index), NDRE (normalized difference red edge), TRRVI (transformed red range vegetation index). PRE (preharvest), POST (postharvest). SI means signal intensity, CV coefficient of variation and S sensitivity (n = 6).

By contrast, NDVI and DVI provided a higher S in postharvest than in preharvest mainly because of the low CV exhibited in the postharvest flights compared with that shown in preharvest (Table 1). NDVI was the most sensitive remote indicator to both irrigation treatments in postharvest, followed by NDRE, TRRVI, OSAVI, and DVI showing similar sensitivity to Ψ_s and being twice as sensitive as MDS.

3.3. Relationship between Plant Water Status Indicators and Vegetation Indices

The relationship between water status indicators and VI was examined by linear correlation analysis. The response of NDVI, OSAVI, DVI, and NDRE at two phenological moments (preharvest and postharvest) was compared in the CTL trees (Figure 4).

VI were more strongly related to Ψ_s in postharvest than in preharvest, when no relationship was found (Figure 4). VI were not able to clearly identify slight differences within the same year in CTL trees, neither 2017, nor 2018; however, VI identified that CTL trees in 2017 showed lower values of Ψ_s than in 2018. NDVI was the index which best fitted with Ψ_s in 2017 (r^2 = 0.55). In 2018, VI were less related to Ψ_s, and NDVI and NDRE resulted in similar, and poor, linear relationships to Ψ_s (r^2 = 0.33 and 0.27, respectively). On the other hand, OSAVI and DVI showed no relationship at both times. In the postharvest baseline of NDVI (Figure 4), it can be observed that there is a clear difference between the measurements taken in 2017 and 2018, and when both years were considered the relationship between Ψ_s and NDVI became stronger (r^2 = 0.78). Differences in environmental water demand and

rainfall patterns during the summer of both years (Figure 1) were reflected in the water stress indicators response during postharvest. On the day of the postharvest flight in 2017, the daily mean VPD was 2.2 kPa, almost 30% higher than that recorded on the day of the postharvest flight in 2018; consequently, VI mean values in the postharvest of 2017 were 17% lower than those computed in 2018.

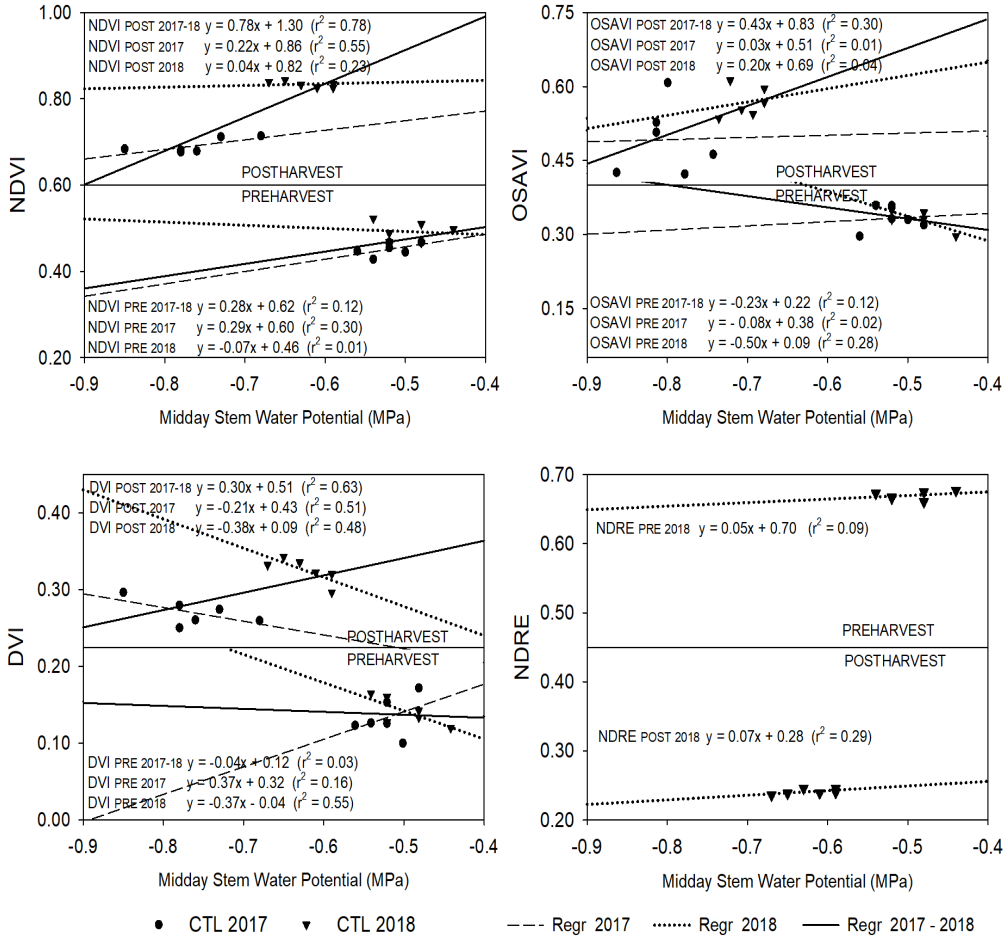

Figure 4. Linear relationships between midday stem water potential and NDVI (normalized difference vegetation index), OSAVI (optimized soil adjusted vegetation index), DVI (difference vegetation index), and NDRE (normalized difference red edge) in CTL trees.

Similarly, when data of all treatments were pooled (Figure 5), NDVI in preharvest still showed no relationship with Ψ_s (r^2 = 0.07), and, while the relationship found was also strong (r^2 = 0.67) in postharvest, the equation obtained was statistically different (according to the ANCOVA analysis) from that obtained only for the CTL treatment (Figures 4 and 5A,B). When both regression lines were compared with the slopes obtained for the relationship between NDVI and Ψ_s, significant differences were observed (p-value = 0.0017). In the case of NDRE vs. Ψ_s, the ANCOVA analysis showed no difference between the slopes or intercepts of the regression lines, and for the measurements taken in postharvest, the relationship increased from r^2 = 0.29 to 0.54 (Figures 4 and 5E). The relationship between DVI and Ψ_s in postharvest remained poor despite the addition of the RDI treatments (Figure 5D); however, OSAVI, which resulted poorly related with Ψ_s in postharvest when only CTL trees were considered, slightly improved the relationship with Ψ_s when all treatments were included, from r^2 = 0.30 to 0.41 (Figure 5C). As regards the postharvest flight, NDVI showed a relationship with Ψ_s that was slightly stronger than that of NDRE and higher than those of OSAVI, TRRVI, and DVI which showed similar results (r^2 = 0.4 Figure 5C,D,F). The relationship between the remote indices and the continuous plant-based water stress indicator, MDS, was lower than with Ψ_s, while NDRE showed a similar coefficient of determination to NDVI (Figure 5G,H).

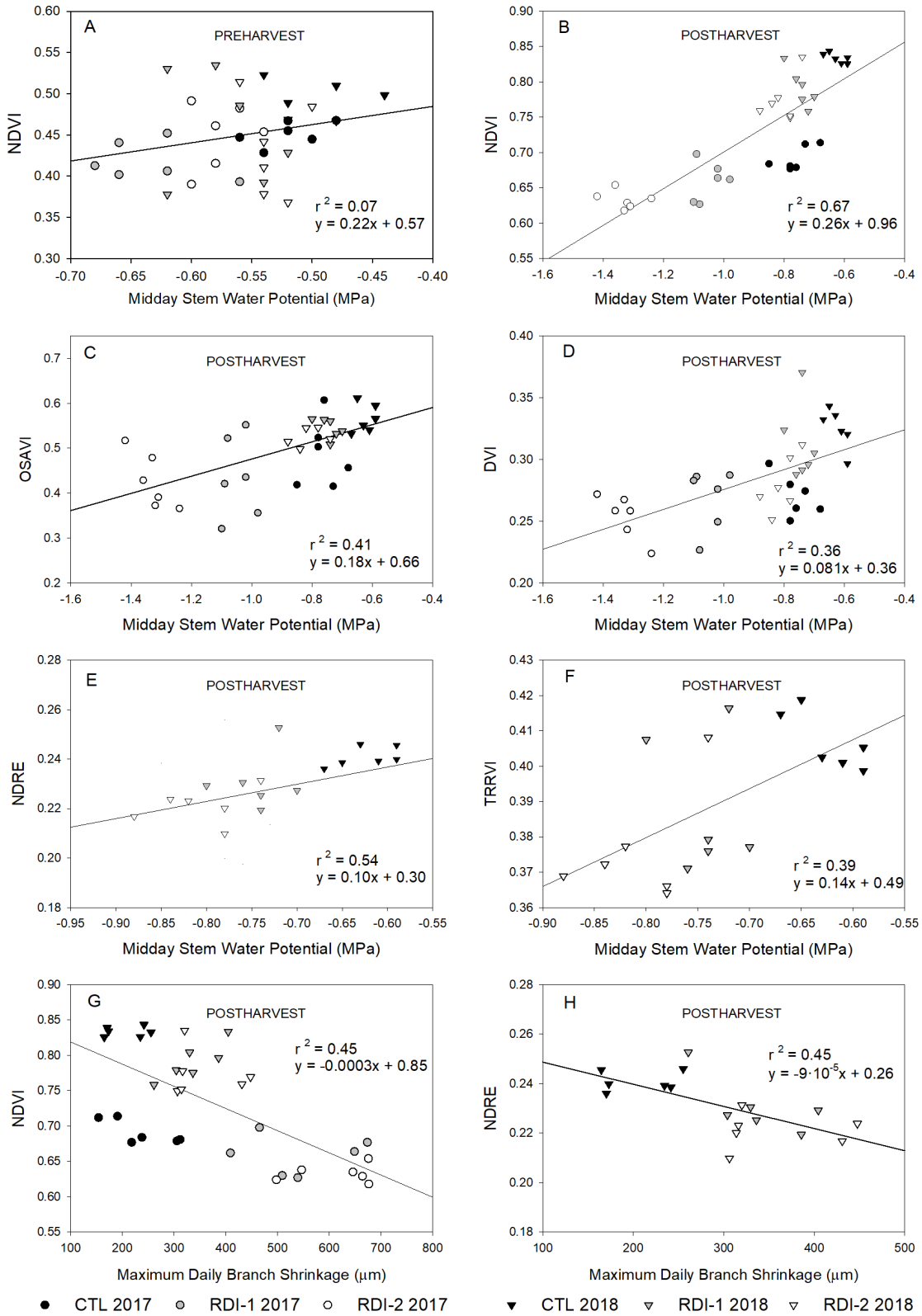

Figure 5. Linear relationships between midday stem water potential and NDVI (normalized difference vegetation index) (**A**,**B**), OSAVI (optimized soil adjusted vegetation index) (**C**), DVI difference vegetation index (**D**), NDRE (normalized difference red edge) (**E**), and TRRVI (transformed red range vegetation index) (**F**). Linear relationships between maximum daily branch shrinkage and NDVI (**G**) and NDRE (**H**).

Figure 6 shows the relationship between the VI and the conventional and continuous indicators Ψ_s and MDS. It was observed that, in general, VI were more strongly related to Ψ_s than to MDS in both 2017 and 2018. Furthermore, it could be seen that the relationships increased in 2017 and decreased in 2018, which would be due to the greater range of values measured in 2017, as RDI trees experienced greater stress in 2017 than in 2018. According to the coefficients of determination obtained, the indices that were most strongly related to Ψ_s and MDS were NDVI and NDRE ($r^2 \cong 0.50$) followed by TRRVI and OSAVI ($r^2 \cong 0.30$), and lastly by DVI ($r^2 \cong 0.20$) and NIR ($r^2 \cong 0.15$).

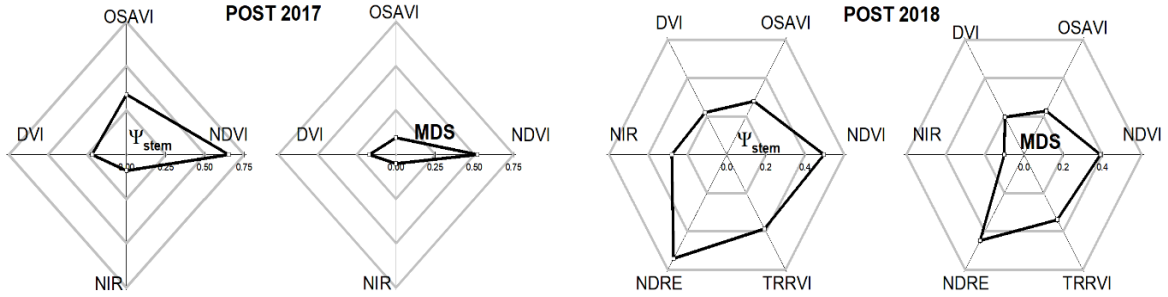

Figure 6. Coefficients of determination obtained from linear relationships between Ψ_s (midday stem water potential) and MDS (maximum daily branch shrinkage) with NDVI, OSAVI, DVI, NDRE, TRRVI, and NIR in 2017 and 2018 postharvest.

3.4. Assessment of Tree Vigor Using Remote Indices

Increases in water stress in sweet cherry trees are closely linked to lower vegetative growth, so, pruning wood mass produced by each tree might be a good indicator of the vegetative growth of the trees and the tree vigor. In our case, the pruning wood mass for both years resulted in a mean value of 9.39 ± 0.78 kg tree^{-1}, with significant differences among treatments (p-value = 0.011), years (p-value < 0.001), and their interaction (p-value < 0.021). Trees under RDI treatments exhibited significantly lower pruning wood mass than CTL trees both years of the study, and trees showed more vegetative growth and consequently more pruning wood mass in 2018 than in 2017. Thus, the values obtained for each tree by the remote VI during postharvest were linearly related with the pruning wood mass of the same tree (Figure 7).

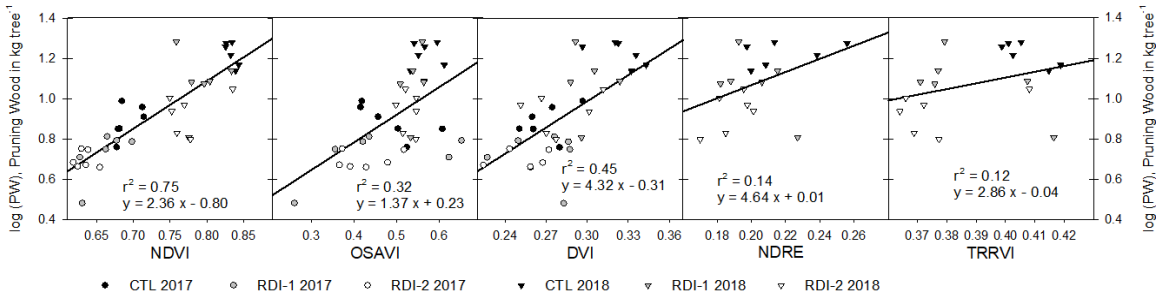

Figure 7. Linear relationships between the logarithm of the pruning wood mass (log (PW)) and postharvest values of remote indicators NDVI (normalized difference vegetation index), OSAVI (optimized soil adjusted vegetation index), DVI (difference vegetation index), NDRE (normalized difference red edge), and TRRVI (transformed red range vegetation index).

Since the pruning wood mass had an asymmetric distribution, the relationships were calculated with its logarithm (log (PW) as the logarithm of the pruning wood mass). Linear regression analysis pointed to a positive and strong relationship between NDVI and log (PW), $r^2 = 0.75$, Figure 7. In the same vein, OSAVI and DVI also showed a positive trend between measurements and vegetative growth, although it was weaker than that obtained with NDVI. For their part, TRRVI and NDRE

measurements were poorly related with log (PW) despite the excellent results obtained by NDRE as water stress detector (Figure 4).

3.5. Tree Yield Estimation

There was no significant effect of the irrigation treatment on tree yield. The mean yield value at harvest was 42 kg tree^{-1} in 2018, a year that was considered a medium-high cropping year in 'Prime Giant'/SL64 sweet cherry trees. Thus, from the data of all trees, a decision tree (DT) model and an artificial neural network (ANN) approach were proposed in order to classify and estimate tree yield.

Both DT and ANN models used the plant-based remote indicators as predictor variables and the amount of cherries produced as the response variable. The mean values of the remote indicators in the 80 trees considered are shown in Table 2.

Table 2. Mean values and standard error of yield and remote plant vegetation indices.

	NDVI	OSAVI	DVI	NDRE	TRRVI	NIR	Yield (kg tree^{-1})
Mean	0.466	0.590	0.140	0.663	0.245	0.589	42.112
SE	0.007	0.007	0.002	0.002	0.001	0.006	1.119

Remote vegetation indices: NDVI (normalized difference vegetation index), OSAVI (optimized soil adjusted vegetation index), DVI (difference vegetation index), NDRE (normalized difference red edge), TRRVI (transformed red range vegetation index), NIR (near-infrared). (n = 80).

With the aim of designing a DT to estimate whether the tree crop load is going to be higher than usual and so more personnel will be required for harvesting, a threshold value was set at 40 kg tree^{-1}. High cropping years necessitate more personnel to hand pick the cherries early in their commercial ripeness state and when market prices are higher. The DT aimed to identify two categories: above and below 40 kg tree^{-1}. Figure 8 shows the resulting DT, which identifies three constraints for the three remote indicators NIR, TRRVI, and NDVI. When the decision tree model was evaluated, it showed a training error of 0.228 and correctly identified 20 trees out of 23 (testing sample). When the confusion matrix was obtained for the testing sample, the precision was 0.870, the recall 0.778, and the true positive rate (specificity) 0.929.

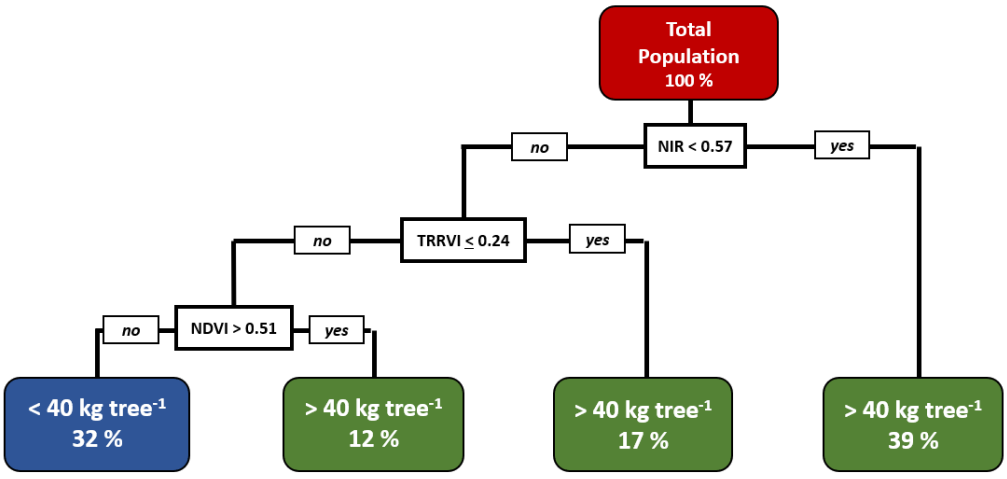

Figure 8. Decision tree analysis for sweet cherry trees classified according to their yield in two situations (higher and lower than 40 kg tree^{-1}) considering mean preharvest value of tree's NIR (near-infrared), TRRVI (transformed red range vegetation index), and NDVI (normalized difference vegetation index) computed in 2018 preharvest.

Similarly, an ANN model to predict the sweet cherry yield of each tree based on the interaction among the remote sensing indicators is proposed. After validation of the methodology to generate prediction models, average values of r^2 = 0.63 and RMSE = 6.05 kg tree^{-1} were obtained. Figure 9 presents a particular case of the relationship between actual and predicted yield obtained by the proposed methodology. As can be seen, there was a strong linear relationship between them. The regression analysis pointed to a good fit (r^2 = 0.67; RMSE = 5.38 kg tree^{-1}) between actual and predicted values. Furthermore, the slope of the regression line obtained was close to a 1:1 line.

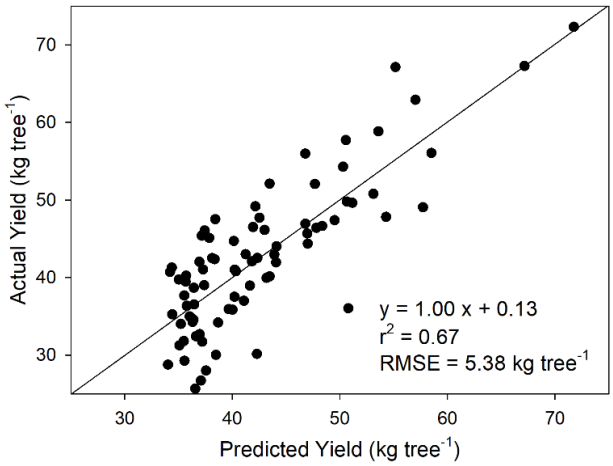

Figure 9. Regression equation obtained for the predicted and the actual yield of sweet cherry trees.

The results of a statistical analysis of both predicted and actual yield are shown in Table 3. Actual and predicted data had similar mean and maximum values and a CV close to 20%. Regarding the distribution of frequencies, both showed a similar trend towards a positive skew (platykurtic dome-shaped trajectory) which, in the case of the predicted tended towards normal (both had Skewness higher than zero and Kurtosis lower than 3). The greatest limitation of the model concerned the minimum values predicted for those sweet cherry trees whose production was between 25 and 34 kg, meaning that the calculation overestimates the yield of those trees with low crop loading (Figure 9).

Table 3. Summary statistics of actual and predicted sweet cherry trees yield distribution.

Yield kg tree^{-1}	Min	Max	Mean	SD	CV (%)	Skewness	Kurtosis
Actual	25.67	72.32	42.46	9.40	22.15	0.83	1.01
Predicted	34.02	71.74	42.47	7.69	18.16	1.49	2.48

Min, minimum value; Max, maximum value; SD, standard deviation; CV, coefficient of variation; normality tests Skewness and Kurtosis.

4. Discussion

The results presented in this work showed that remote vegetation indices derived from UAS imagery can successfully assess sweet cherry tree water status; however, these indicators were not as sensitive as conventional and continuous indicators for showing significant differences among irrigation treatments when a slight water stress is applied. In general, remote indices led to significant differences in postharvest, when severe water deficit was applied in the RDI treatments. In preharvest, TRRVI was the only remote index which identified the slight water deficit applied to RDI-1, pointing to significant differences with CTL (Figure 3L). As the vegetative growth period of sweet cherry trees lasts longer than fruit development, the measurements obtained during preharvest from the NDVI, DVI, OSAVI, and TRRVI resulted in lower values than in postharvest. By contrast, the NDRE index was lower during postharvest [9]. In August, when the postharvest flights took place, sweet cherry

trees have already reached their maximum leaf area, while during preharvest (June), although canopy development overlaps fruit growth (spur leaves) the maximum canopy development in early cultivars such as 'Prime Giant' is reached in postharvest [42,43].

NDVI was the most sensitive VI of all the remote indicators studied in sweet cherry trees during postharvest, and clearly reflected the result of cumulative water deficits. NDVI was able to distinguish between both RDI treatments and it resulted to have a high sensitivity (Table 1). Indeed, NDVI has been successfully employed in vines to identify different irrigation treatments [2,44]. Our results showed that CTL trees had higher NDVI values than RDI trees as water-stress reduces the capacity of plants to absorb the red energy and reflect NIR. These results are contrary to those reported in apricot trees by Ballester et al. [45], who found higher sensitivity for remote VI based on OSAVI measurements than in NDVI. This might be explained by the fact that the NIR spectral band has been stronger related than any other spectral band with variations in leaf turgidity and canopy structure [46]. In sweet cherry trees, one of the physical mechanisms that first appears in the face of water stress is leaf curling [47]. Such changes in leaf turgidity may lead to NDVI acting as a better water stress detention index in sweet cherry trees than in other fruit trees, whose leaves do not curl so readily. In our study in sweet cherry trees, DVI and OSAVI showed the highest noise of all the remote indicators during preharvest and postharvest, respectively, which decreased its sensitivity (Table 1).

Despite the strong signal intensity of NDVI in both pre- and postharvest periods, it had a high CV in preharvest, meaning that its sensitivity was lower than that obtained by NDRE and TRRVI. However, by postharvest, tree foliage had completely developed and so the CV decreased and NDVI sensitivity increased. The differences described between the preharvest and the postharvest measurements of NDVI are similar to those reported by Bellvert et al. [48] in almond and pistachio trees. Similarly to NDVI, the sensitivity of the NIR spectral band also increased in postharvest. The NIR response is directly related to canopy leaf temperature variations, and water-stressed canopies are warmer than those of well-watered trees, as leaf temperature rises when the stomata close [49]. Thus, the water deficit applied to RDI trees in postharvest led to a stomata closure.

When all the remote indicators were compared with conventional and continuous indicators (Figure 6), NDVI showed a strong relationship with Ψ_s, higher than that mentioned by Zhao et al. [5] in almond trees and lower than that reported by Beeri et al. [50] in citrus and almond trees. Ψ_s has been described as the most reliable water stress indicator for assessing water status in sweet cherry trees [15,16]. Consequently, we considered the response of the trees and the relationship between each remote VI and Ψ_s in order to assess their usefulness detecting changes caused by the water stress in the canopy structure. The relationship between NDVI and Ψ_s was stronger when all treatments were considered (Figure 5) than when only the CTL treatment was considered (Figure 4). Furthermore, the relationship was even stronger when all data (2017 and 2018) were taken into account. Neither NDVI, nor any other VI were able to distinguish the small variation measured by Ψ_s in CTL trees (Figure 4). NDRE and OSAVI also exhibited a strong relationship with Ψ_s, the former showing similar coefficient of determination than that showed in pear trees by Van Beek [51]. As regards the relationship between NDVI and NDRE with MDS, it was similar for both VI and lower than that obtained with Ψ_s (Figure 5G,H and Figure 6). It was not possible to determine the threshold value above which NDVI is not linearly related with MDS.

NDVI was also the remote VI with the strongest relationship with tree biomass, measured as pruning wood mass, followed by DVI, OSAVI, NDRE, and TRRVI (Figure 7). This relationship agrees with the results of Conesa et al. [10] and Matese and Di Genaro [52] in nectarine and 'Sangiovese' grapes, respectively, who found solid relationships between the NDVI computed in a tree and the pruning wood mass produced by it.

Concerning crop yield estimates, the positive results of both DT and ANN obtained by the combination of remote sensing indices highlight the usefulness of UAS imagery for yield prediction in sweet cherry trees. Using both DT and ANN methodologies is not redundant, since each complements and nurtures the other.

The DT predictive model showed that NIR, TRRVI, and NDVI indices played a determining role in the classification of tree yield. The results obtained for the confusion matrix and the precision of 0.87, show that the proposed model is a robust method and explains why it has previously been used with good success to predict fruit yield in other fruit trees, such as apple [53]. There were no significant differences among the irrigation treatments in terms of fruit yield, although the results demonstrated that trees with a high NDVI had fruit yields above 40 kg tree^{-1} (Figure 8). Higher NDVI values during preharvest are not necessarily related to higher postharvest vegetative growth, since CTL trees had higher vegetative growth and pruning wood than RDI trees. High values of NDVI in RDI trees during preharvest could be linked to a trend previously reported in sweet cherry trees submitted to water stress—that their leaf area is greater initially due to a higher number of spurs per meter; however, in postharvest the pruning wood mass of RDI trees was lower as a result of the lower growth of current the season's extension shoots compared to CTL trees [42].

As regards the ANN, the proposed methodology explained 67% of the variation in fruit yield in 2018, a year in which trees showed highly variable crop load values. The distribution of actual and predicted yields did not differ markedly (Table 3), but the approach applying ANN was not able to predict fruit yield in those trees with crop loads under 35 kg tree^{-1} (Figure 9). Although this could be considered a major restriction of the method, the greatest problem in sweet cherry trees occurs when the fruit yield exceeds 40 kg tree^{-1} and the needs of fruit-pickers increases. However, it could still be considered an effective model. Nevertheless, the proposed approaches are based on only one year, so further analysis is needed and the model proposed might be a good starting point for future works. Thus, the use of ANN for predicting fruit yield based on airborne hyperspectral imagery in sweet cherry trees provided promising results as has already been reported in other fruit trees, such as mango, avocado, and apple [25,46,54].

5. Conclusions

The remote VI studied were sensitive to the changes in the canopy of the sweet cherry trees caused by water deficit; however, they were not sensitive enough to detect small tree-to-tree variations within the same irrigation treatment. Moreover, they showed different results according to their phenological stage. In preharvest, when tree canopies were not completely developed none of the remote indicators studied resulted in strong correlation with Ψ_s. When we compared the results of VI in postharvest, when leaf area is completely developed, NDVI, NDRE, and TRRVI were able to distinguish between the trees of CTL and RDI; however, NDVI was the only VI able to differentiate between trees of RDI-1 and RDI-2, resulting in the highest sensitivity ($S > 22$) and was the indicator which resulted in the strongest relationship with Ψ_s ($r^2 = 0.60$). Our results underline the utility of NDVI as a VI in sweet cherry trees.

The predictive models proposed provide growers with more accurate information on sweet cherry tree yield. The decision tree obtained showed a precision of 0.87 when classifying the trees according to their yield, and the application of artificial neuronal networks explained 67% of the variation in fruit yield. The use of both models has positive implications for predicting high crop loads, planning the need for personnel and for scheduling optimal harvesting times.

Author Contributions: Conceptualization, V.B., P.J.B.-R., R.T.-S. and R.D.; methodology, V.B., P.J.B.-R., C.C. and R.D.; software, R.T.-S. and F.S.-V.; validation, V.B., P.J.B.-R., C.C. and R.D.; formal analysis, V.B., P.J.B.-R. and C.C.; investigation, V.B., P.J.B.-R., C.C.; F.S.-V., R.T.-S. and R.D.; resources, C.C.; F.S.-V., R.T.-S. and R.D.; data curation, V.B., P.J.B.-R. and C.C.; writing—original draft preparation, V.B. and P.J.B.-R.; writing—review and editing, R.D. and R.T.-S.; visualization, V.B., C.C.; supervision, V.B., R.D.; project administration, R.T.-S. and R.D.; funding acquisition, R.T.-S. and R.D. All authors have read and agreed to the published version of the manuscript.

Funding: This research was funded by the Spanish Economy and Competitiveness Ministry (MINECO) and the European Agricultural Funds for Rural Development. Reference: AGL2013-49047-C2-1-R, AGL2016-77282-C33-R and the "Fundación Séneca, Agencia de Ciencia y Tecnología" of the Region of Murcia under the Excellence Group Program 19895/GERM/15. Victor Blanco acknowledges the research initiation grant received from the Technical University of Cartagena (UPCT).

Acknowledgments: The authors are grateful to Pedro and Agustín Carrión-Guardiola, "Finca Toli" farm owners, for letting them use their facilities to carry out the tests.

Conflicts of Interest: The authors declare no conflict of interest.

References

1. Cammarano, D.; Fitzgerald, G.J.; Casa, R.; Basso, B. Assessing the Robustness of Vegetation Indices to Estimate Wheat N in Mediterranean Environments. *Remote Sens.* **2014**, *6*, 2827–2844. [CrossRef]
2. Cancela, J.J.; Fandiño, M.; Rey, B.J.; Dafonte, J.; González, X.P. Discrimination of irrigation water management effects in pergola trellis system vineyards using a vegetation and soil index. *Agric. Water Manag.* **2017**, *183*, 70–77. [CrossRef]
3. Gago, J.; Douthe, C.; Coopman, R.E.; Gallego, P.P.; Ribas-Carbo, M.; Flexas, J.; Escalona, J.; Medrano, H. UAVs challenge to assess water stress for sustainable agriculture. *Agric. Water Manag.* **2015**, *153*, 9–19. [CrossRef]
4. Zhang, L.; Zhang, H.; Niu, Y.; Han, W. Mapping Maize Water Stress Based on UAV Multispectral. *Remote Sens.* **2019**, *11*, 605. [CrossRef]
5. Zhao, T.; Stark, B.; Chen, Y.Q.; Ray, A.; Doll, D. More Reliable Crop Water Stress Quantification Using Small Unmanned Aerial Systems (sUAS). *IFAC Pap.* **2016**, *49*, 409–414. [CrossRef]
6. Rouse, J.W.; Haas, R.H.; Schell, J.A.; Deering, D.W. Monitoring vegetation systems in the great plains with ERTS. In *Third ERTS-1 Symposium*; NASA: Washington, DC, USA, 1973; Volume 1, pp. 309–317.
7. Rondeaux, G.; Steven, M.; Baret, F. Optimization of soil-adjusted vegetation indices. *Remote Sens. Environ.* **1996**, *55*, 95–107. [CrossRef]
8. Tucker, C.J. Red and photographic infrared linear combinations for monitoring vegetation. *Remote Sens. Environ.* **1979**, *8*, 127–150. [CrossRef]
9. Barnes, E.M.; Clarke, T.R.; Richards, S.E.; Colaizzi, P.D.; Haberland, J.; Kostrzewski, M.; Waller, P.; Choi, C.; Riley, E.; Thompson, T.; et al. Coincident Detection of Crop Water Stress, Nitrogen Status and Canopy Density Using Ground Based Multispectral Data. In *Proceedings of the Fifth International Conference on Precision Agriculture, 16–19 July 2000, Bloomington, MN, USA*; Robert, P.C., Rust, R.H., Larson, W.E., Eds.; ASA, CSSA and SSA: Madison, WI, USA, 2000; pp. 1–15.
10. Conesa, M.R.; Conejero, W.; Vera, J.; Ramírez-Cuesta, J.M.; Ruiz-Sánchez, M.C. Terrestrial and Remote Indexes to Assess Moderate Deficit Irrigation in Early-Maturing Nectarine Trees. *Agronomy* **2019**, *9*, 630. [CrossRef]
11. Gonzalez-Dugo, V.; Zarco-Tejada, P.J.; Nicolas, E.; Nortes, P.A.; Alarcón, J.J.; Intrigliolo, D.S.; Fereres, E. Using high resolution UAV thermal imagery to assess the variability in the water status of five fruit tree species within a commercial orchard. *Precis. Agric.* **2013**, *14*, 660–678. [CrossRef]
12. Santesteban, L.G.; Di Gennaro, S.F.; Herrero-Langreo, A.; Miranda, C.; Royo, J.B.; Matese, A. High-resolution UAV-based thermal imaging to estimate the instantaneous and seasonal variability of plant water status within a vineyard. *Agric. Water Manag.* **2017**, *183*, 49–59. [CrossRef]
13. Stagakis, S.; González-Dugo, V.; Cid., P.; Guillén-Climent, M.L.; Zarco-Tejada, P.J. Monitoring water stress and fruit quality in an orange orchard under regulated deficit irrigation using narrow-band structural and physiological remote sensing indices. *ISPRS J. Photogramm.* **2012**, *71*, 47–61. [CrossRef]
14. Blando, F.; Oomah, B.D. Sweet and sour cherries: Origin, distribution, nutritional composition and health benefits. *Trends Food Sci. Tech.* **2019**, *86*, 517–529. [CrossRef]
15. Blanco, V.; Torres-Sánchez, R.; Blaya-Ros, P.J.; Pérez-Pastor, A.; Domingo, R. Vegetative and reproductive response of 'Prime Giant' sweet cherry trees to regulated deficit irrigation. *Sci. Hortic.* **2019**, *249*, 478–489. [CrossRef]
16. Marsal, J.; Lopez, G.; del Campo, J.; Mata, M.; Arbones, A.; Girona, J. Postharvest regulated deficit irrigation in 'Summit' sweet cherry fruit yield and quality in the following season. *Irrig. Sci.* **2010**, *28*, 181–189. [CrossRef]
17. Carrasco-Benavides, M.; Espinoza Meza, S.; Olguín-Cáceres, J.; Muñoz-Concha, D.; von Bennewitz, E.; Ávila-Sánchez, C.; Ortega-Farías, S. Effects of regulated post-harvest irrigation strategies on yield, fruit quality and water productivity in a drip-irrigated cherry orchard. *N. Z. J. Crop. Hort.* **2020**, *48*, 97–116. [CrossRef]

18. Abdelfatah, A.; Aranda, X.; Savé, R.; de Herralde, F.; Biel, C. Evaluation of the response of maximum daily shrinkage in young cherry trees submitted to water stress cycles in a greenhouse. *Agric. Water Manag.* **2013**, *118*, 150–158. [CrossRef]
19. Blanco, V.; Domingo, R.; Pérez-Pastor, A.; Blaya-Ros, P.J.; Torres-Sánchez, R. Soil and plant water indicators for deficit irrigation management of field-grown sweet cherry trees. *Agric. Water Manag.* **2018**, *208*, 83–94. [CrossRef]
20. Livellara, N.; Saavedra, F.; Salgado, E. Plant based indicators for irrigation scheduling in young cherry trees. *Agric. Water Manag.* **2011**, *98*, 684–690. [CrossRef]
21. Ortuño, M.F.; Alarcón, J.J.; Nicolás, E.; Torrecillas, A. Interpreting trunk diameter changes in young lemon trees under deficit irrigation. *Plant Sci.* **2004**, *167*, 275–280. [CrossRef]
22. Puerto, P.; Domingo, R.; Torres, R.; Pérez-Pastor, A.; García-Riquelme, M. Remote management of deficit irrigation in almond trees based on maximum daily trunk shrinkage. Water relations and yield. *Agric. Water Manag.* **2013**, *126*, 33–45. [CrossRef]
23. Aggelopoulou, K.D.; Wulfsohn, D.; Fountas, S.; Gemtos, T.A.; Nanos, G.D.; Blackmore, S. Spatial variation in yield and quality in a small apple orchard. *Precis. Agric.* **2009**, *11*, 538–556. [CrossRef]
24. Mu, Y.; Fujii, Y.; Takata, D.; Zheng, K.N.; Honda, K.; Ninomiya, S.; Guo, W. Characterization of peach tree crown by using high-resolution images from an unmanned aerial vehicle. *Hortic. Res.* **2018**, *74*, 5. [CrossRef] [PubMed]
25. Rahman, M.M.; Robson, A.; Bristow, M. Exploring the Potential of High Resolution WorldView-3 Imagery for Estimating Yield of Mango. *Remote Sens.* **2018**, *10*, 1866. [CrossRef]
26. Whiting, M.D.; Perry, R.L. Chapter 18: Fruit Harvest Methods and Technologies. In *Cherries: Botany, Production and Uses*, 1st ed.; Quero-García, J., Iezzoni, A., Pulawska, J., Lang, G., Eds.; CABI: Oxfordshire, UK, 2017; pp. 442–459.
27. Lee, B.-H.; Kendel, P.; Brorsen, B.W. Pre-harvest forecasting of county wheat yield and wheat quality using weather information. *Agric. For. Meteorol.* **2013**, *15*, 26–35. [CrossRef]
28. Goldstein, A.; Fink, L.; Meitin, A.; Bohadana, S.; Lutenberg, O.; Ravid, G. Applying machine learning on sensor data for irrigation recommendations: Revealing the agronomist's tacit knowledge. *Precis. Agric.* **2018**, *19*, 3. [CrossRef]
29. Navarro-Hellín, H.; Martínez-del-Rincon, J.; Domingo-Miguel, R.; Soto-Valles, F.; Torres-Sánchez, R. A decision support system for managing irrigation in agriculture. *Comput. Electron. Agric.* **2016**, *124*, 121–131. [CrossRef]
30. Romero, M.; Luo, Y.; Su, B.; Fuentes, S. Vineyard water status estimation using multispectral imagery from an UAV platform and machine learning algorithms for irrigation scheduling management. *Comput. Electron. Agric.* **2018**, *147*, 109–117. [CrossRef]
31. Torres, R.; Navarro-Hellin, H.; Frutos, A.G.; Ruiz-Abellon, M.C.; Domingo, R. A Decision Support System for Irrigation Management: Analysis and Implementation of Different Learning Techniques. *Water* **2020**, *12*, 548. [CrossRef]
32. Allen, R.G.; Pereira, L.S.; Raes, D.; Smith, M. FAO Irrigation and drainage paper 56. In *Crop Evapotranspiration-Guidelines for Computing Crop Water Requirements*; Food and Agriculture Organization: Rome, Italy, 1998.
33. Marsal, J. FAO irrigation and drainage paper 66. Sweet Cherry. In *Crop Yield Response to Water*; Food and Agriculture Organization: Rome, Italy, 2012; pp. 449–457.
34. Fereres, E.; Martinich, D.A.; Aldrich, T.M.; Castel, J.R.; Holzapfel, E.; Schulbach, H. Drip irrigation saves money in young almond orchards. *Calif. Agric.* **1982**, *36*, 12–13.
35. McCutchan, H.; Shackel, K.A. SWP as a sensitive indicator of water stress in prune trees (*Prunusdomestica* L. cv. French). *J. Am. Soc. Hortic. Sci.* **1992**, *117*, 607–611. [CrossRef]
36. Gholipoor, M.; Nadali, F. Fruit yield prediction of pepper using artificial neural network. *Sci. Hortic.* **2019**, *250*, 249–253. [CrossRef]
37. Fernandes, J.L.; Ebecken, N.F.F.; Esquerdo, J.C.D.M. Sugarcane yield prediction in Brazil using NDVI time series and neural networks ensemble. 2017. *Int. J. Remote Sens.* **2011**, *38*, 4631–4644. [CrossRef]
38. Veenadhari, S.; Mishra, B.; Singh, C.D. Soybean Productivity Modelling using Decision Tree Algorithms. *Int. J. Comp. Appl.* **2011**, *27*, 11–15. [CrossRef]

39. Bhatnagar, R.; Gohain, G.B. Crop Yield Estimation Using Decision Trees and Random Forest Machine Learning Algorithms on Data from Terra (EOS AM-1) & Aqua (EOS PM-1) Satellite Data. In *Machine Learning and Data Mining in Aerospace Technology. Studies in Computational Intelligence*, 1st ed.; Hassanien, A., Darwish, A., El-Askary, H., Eds.; Springer Int. Publishing: Cham, Switzerland, 2020; pp. 107–124.
40. San-Segundo, R.; Navarro-Hellín, H.; Torres-Sánchez, R.; Hodgins, J.; de la Torre, F. Increasing robustness in the detection of freezing of gait in Parkinson's disease. *Electronics* **2019**, *8*, 119. [CrossRef]
41. Goldhamer, D.A.; Fereres, E. Irrigation scheduling protocols using continuously recorded trunk diameter measurements. *Irrig. Sci.* **2001**, *20*, 115–125. [CrossRef]
42. Blanco, V.; Blaya-Ros, P.J.; Torres-Sánchez, R.; Domingo, R. Influence of Regulated Deficit Irrigation and Environmental Conditions on Reproductive Response of Sweet Cherry Trees. *Plants.* **2020**, *9*, 94. [CrossRef]
43. Lauri, P.E.; Claverie, J. Sweet Cherry Tree Architecture, Physiology and Management: Towards an Integrated View. *Acta Hort.* **2008**, *667*, 361–366. [CrossRef]
44. Baluja, J.; Diago, M.P.; Balda, P.; Zorer, R.; Meggio, F.; Morales, F.; Tardaguilla, J. Assessment of vineyard water status variability by thermal and multispectral imagery using an unmanned aerial vehicle (UAV). *Irrig. Sci.* **2012**, *30*, 511–522. [CrossRef]
45. Ballester, C.; Zarco-Tejada, P.J.; Nicolás, E.; Alarcón, J.J.; Fereres, E.; Intrigliolo, D.S.; Gonzalez-Dugo, V. Evaluating the performance of xanthophyll, chlorophyll and structural-sensitive spectral indices to detect water stress in five fruit tree species. *Prec. Agric.* **2018**, *19*, 178–193. [CrossRef]
46. Robson, A.; Rahman, M.M.; Muir, J. Using WorldView Satellite Imagery to Map Yield in Avocado (*Perseaamericana*): A Case Study in Bundaberg, Australia. *Remote Sens.* **2017**, *9*, 1223. [CrossRef]
47. Vossen, P.M.; Silva, D. Chapter 16. Temperate Tree Fruit and Nut Crops. In *California Master Gardener Handbook*, 2nd ed.; Pittenger, D.R., Ed.; University of California, Pub.: Davis, CA, USA, 2015; Volume 3382, pp. 83–108.
48. Bellvert, J.; Adeline, K.; Baram, S.; Pierce, L.; Sanden, B.L.; Smart, D.R. Monitoring Crop Evapotranspiration and Crop Coefficients over an Almond and Pistachio Orchard Throughout Remote Sensing. *Remote Sens.* **2018**, *10*, 2001. [CrossRef]
49. Virlet, N.; Lebourgeois, V.; Martinez, S.; Costes, E.; Labbé, S.; Regnard, J.L. Stress indicators based on airborne thermal imagery for field phenotyping a heterogeneous tree population for response to water constraints. *J. Exp. Bot.* **2014**, *65*, 5429–5442. [CrossRef] [PubMed]
50. Beeri, O.; Mey-tal, S.; Raz, Y.; Rud, R.; Pelta, R. Detecting variability in plant water potential with multi-spectral satellite imagery. In Proceedings of the 14th International Conference on Precision Agriculture, Montreal, QC, Canada, 24–27 June 2018; International Society of Precision Agriculture, Pub.: Monticello, IL, USA, 2018.
51. Van Beek, J.; Tits, L.; Somers, B.; Coppin, P. Stem Water Potential Monitoring in Pear Orchards through WorldView-2 Multispectral Imagery. *Remote Sens.* **2013**, *5*, 6647–6666. [CrossRef]
52. Matese, A.; Di Gennaro, S.F. Practical Applications of a Multisensor UAV Platform Based on Multispectral, Thermal and RGB High Resolution Images in Precision Viticulture. *Agriculture* **2018**, *8*, 116. [CrossRef]
53. Papageorgiou, E.I.; Aggelopoulou, K.D.; Gemtos, T.A.; Nanos, G.D. Yield prediction in apples using Fuzzy Cognitive Map learning approach. *Comput. Electron. Agric.* **2013**, *91*, 19–29. [CrossRef]
54. Cheng, H.; Damerow, L.; Sun, Y.; Blanke, M. Early Yield Prediction Using Image Analysis of Apple Fruit and Tree Canopy Features with Neural Networks. *J. Imaging.* **2017**, *3*, 6. [CrossRef]